Stability of plane Poiseuille flow of a Bingham fluid through a deformable neo-Hookean channel

Ramkarn Patne and V. Shankar*
Department of Chemical Engineering, Indian Institute of Technology, Kanpur 208016, India

(Received 27 December 2018; published 5 August 2019)

We study the linear stability of plane Poiseuille flow of a Bingham fluid through a deformable neo-Hookean channel. The analysis reveals the existence of a finite-wave instability in the creeping-flow limit, which is absent for Newtonian fluid flow in the same geometry. Indeed, the instability in plane Poiseuille flow of a Bingham fluid closely resembles the finite-wave instability exhibited by plane Couette flow of a Newtonian fluid past a deformable solid. The motion of the unyielded region near the channel centerline effectively results in a Couette-like drag flow of the fluid in the yielded region, albeit with a parabolic base flow velocity profile. More importantly, the boundary conditions at the interface between yielded and unyielded zones is found to be crucial for the existence of the finite-wave instability. This is in stark contrast to Newtonian channel flow where the conditions at the channel centerline are dictated by the symmetry or antisymmetry of the velocity perturbations. The continuation of the predicted instability in the creeping-flow limit is also shown to determine the stability of the flow of a Bingham fluid at higher Reynolds number. In addition to treating the plug as a rigid solid, we also consider the plug to be an elastic solid and show that the elastic nature of the plug does not have any effect on the predicted finite-wave instability. We further argue, using the elastic plug scenario, that some of the regularized models can introduce model-dependent instabilities which are specific to the parameters used in the models.

DOI: 10.1103/PhysRevFluids.4.083302

I. INTRODUCTION

The flow of yield-stress fluids is commonly encountered in the oil industry during drilling and cementing operations, in food processing industries (e.g., mayonnaise) or health care products (e.g., toothpaste), and in polymer industries [1]. These materials show a common characteristic of the requirement of a minimum shear stress below which they behave like a solid while above they flow like a fluid [2,3]. Apart from these industrial applications, biological fluids such as blood exhibit yield-stress-fluid behavior wherein the value of the yield stress depends on its constituents including red blood cells, white blood cells, and blood platelets [4,5].

To mathematically model the behavior of the yield-stress fluids, Bingham [6] proposed a one-dimensional model where it was assumed that the material behaves as a rigid body before yielding and as a Newtonian fluid after yielding. Oldroyd [7] extended the Bingham model to three dimensions by expressing the model in appropriate tensorial form. The modified Bingham model of Oldroyd [7] consists of a plug region, which can be treated either as a rigid body or as an elastic solid, and a yielded region, which is treated as a Newtonian fluid. In the present work we consider both models for the unyielded region, i.e., rigid as well as elastic, and show that the instabilities predicted here do not depend on the model employed for the unyielded region. The linear stability

*Corresponding author: vshankar@iitk.ac.in

TABLE I. Summary of the linearization of the interface conditions in the literature for plane Poiseuille flow of a Newtonian fluid. The second, third, and fourth columns respectively refer to the Taylor expansion of base-state quantities, direction(s) of Taylor expansion, and instabilities predicted as a consequence of the linearization of the interface conditions. Here FW, SW, WM, and IM respectively refer to the finite-wave, short-wave, wall mode, and inviscid mode instabilities. Consistent formulation predicts the existence of short-wave, wall, and inviscid modes for plane Poiseuille flow of a Newtonian fluid through a neo-Hookean channel.

Work	Taylor expanded	Direction of Taylor expansion	Instabilities
Gkanis and Kumar [10]	fluid and solid	normal	FW and SW
Gaurav and Shankar [11]	fluid	normal	SW, low-Re, WM, and IM
Patne *et al.* [12]	fluid	tangential and normal	SW, WM, and IM

of plane Poiseuille flow of a Bingham fluid with a rigid plug was first studied by Frigaard *et al.* [2]. They predicted that the minimum Reynolds number for linear instability increases almost linearly with increasing Bingham number. Nouar *et al.* [8] studied the same problem using the Chebyshev collocation method and predicted that the plane Poiseuille flow of a Bingham fluid is linearly stable. The disagreement between Frigaard *et al.* [2] and Nouar *et al.* [8] was attributed to the erroneous numerical method employed by the former to compute the eigenvalues. Thus, while plane Poiseuille flow of a Newtonian fluid is linearly unstable due to the Tollmien-Schlichting instability [9], it is linearly stable for Bingham fluid flow in a rigid channel. This scenario in rigid channels points to the importance of the yield-stress nature of the fluid on the stability of fluid flows.

The linear stability of plane Poiseuille flow of a Newtonian fluid through a deformable neo-Hookean channel was first studied by Gkanis and Kumar [10] in the creeping-flow limit. Their study predicted the presence of two types of instabilities, viz., a finite-wave instability for which the critical wave number k_c and critical nondimensional shear rate or moving plate velocity Γ_c are less than unity and a short-wave instability characterized by $k_c, \Gamma_c > 1$. Gaurav and Shankar [11] studied the same problem and predicted the existence of an instability at low but nonzero Re in addition to the short-wave instability. However, their study predicted the absence of the finite-wave instability predicted by Gkanis and Kumar [10]. The disagreement between the predictions of Gaurav and Shankar [11] and Gkanis and Kumar [10] was ascribed to the inconsistent interface conditions used by the latter.

Later, Patne *et al.* [12] demonstrated that a consistent way to derive the interface conditions is to Taylor expand fluid base-state quantities in both flow and normal directions provided that the solid and fluid are described in the Lagrangian and Eulerian frameworks, respectively. The aforementioned Taylor expansion gave rise to a term in normal stress balance at the fluid-solid interface which resulted in an interaction between the base-state pressure gradient and perturbations. The effect of the consistent interface conditions so derived on the existing instabilities was analyzed by Patne and Shankar [13], who showed that the low-Re instability predicted by Gaurav and Shankar [11] is absent when the consistent formulation is used. Patne and Shankar [13] predicted three classes of instabilities for plane Poiseuille flow of a Newtonian fluid through a neo-Hookean channel, viz., short-wave mode dominant for $\mathrm{Re} < 1$ and/or $H < 1$ and wall and inviscid modes of instability dominant at high Re with respective scaling laws $\Gamma \sim \mathrm{Re}^{-1/3}$ and $\Gamma \sim \mathrm{Re}^{-1}$. A summary of previous theoretical results concerning the stability of the plane Poiseuille flow through a neo-Hookean channel is shown in Table I. It is worth mentioning that Gkanis and Kumar [10] studied the plane Poiseuille flow through a neo-Hookean channel in the creeping-flow limit only, and thus they did not study the wall modes and inviscid modes which appear when $\mathrm{Re} > 100$.

The studies discussed above analyzed the linear stability of plane Poiseuille flow of either a Bingham fluid past a rigid surface or a Newtonian fluid past a neo-Hookean surface. The effect of the deformable wall on the stability of the flow of a Bingham fluid was not explored therein. Furthermore, Bingham fluids are involved in food processing, petroleum, and oil industries, where

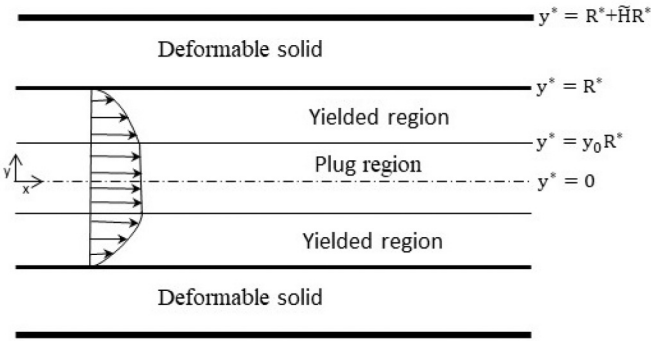

FIG. 1. Schematic of the flow geometry studied in the present work. Here y_0R^* and $\tilde{H}R^*$ are, respectively, the dimensional plug and solid thicknesses. At $y^* = R^* + \tilde{H}R^*$ and $-R^* - \tilde{H}R^*$, the deformable solid is perfectly bonded to a rigid solid.

manipulation of their instabilities is required to achieve processing goals such as mixing, transport, and handling. The instabilities exhibited by the flow of blood, a yield-stress fluid, through a blood vessel (a deformable tube) can also be modeled using the interaction between a Bingham fluid and deformable wall. The present study is also aimed at answering the question as to whether the introduction of a deformable wall can destabilize the plane Poiseuille flow of a Bingham fluid which is linearly stable for flow though a rigid channel [2].

The rest of this paper is organized as follows. In Sec. II we provide the governing equations for the fluid and solid, and the linearized governing differential equations and interface conditions. The key results obtained from our analysis are presented and discussed in Sec. III. Section IV analyzes the effect of considering the elastic nature of the plug on the stability of Bingham fluid flows. The salient conclusions of the present study are summarized in Sec. V.

II. PROBLEM FORMULATION

Patne *et al.* [12] demonstrated the utility of the Lagrangian-three-state formulation for investigating hydrodynamic stability of flows past a neo-Hookean solid; that formulation is used here to study the flow of a Bingham fluid past a neo-Hookean solid. We consider an incompressible Bingham fluid of (limiting) viscosity μ_0^* and density ρ^* flowing through a channel of height $2R^*$, where the asterisk superscript denotes dimensional quantities (see Fig. 1). The channel walls are lined with a neo-Hookean solid of shear modulus G^*, density ρ^*, and thickness $\tilde{H}R^*$. The densities of the deformable solid and the fluid are assumed to be identical in the interest of simplicity. In prior experiments [14,15] involving the flow of water through deformable channels fabricated using polydimethylsiloxane gel, the densities of the fluid and the deformable solid were comparable, and hence the assumption of equal densities in the fluid and solid is a reasonable one. The upper and lower deformable walls are assumed to be perfectly bonded to the rigid solid at $y^* = R^* + \tilde{H}R^*$ and $y = -R^* - \tilde{H}R^*$, respectively. The assumption of the rigid wall constraining the deformable walls is motivated by prior experiments involving Newtonian fluids where typically a polymer gel or an elastomer forms a deformable annular region between the flowing fluid and rigid solid [14,16].

To obtain the base-state velocity profile in the fluid, we proceed as follows. The continuity equation is $\nabla^* \cdot \mathbf{v}^* = 0$. The momentum equation in the yielded region is

$$\rho^* \left[\frac{\partial \mathbf{v}^*}{\partial t^*} + (\mathbf{v}^* \cdot \nabla^*)\mathbf{v}^* \right] = -\nabla^* p^* + \nabla^* \cdot \boldsymbol{\tau}^*. \tag{1}$$

Here $\mathbf{v}^* = (v_x^*, v_y^*, v_z^*)$ is the velocity field, with v_i^* the velocity component in the i direction, where $i = x, y, z$. Also, p^* and $\boldsymbol{\tau}^*$ are, respectively, the dimensional pressure and stress fields in the fluid.

The gradient operator is $\nabla^* = \hat{\mathbf{e}}_\mathbf{x}\frac{\partial}{\partial x^*} + \hat{\mathbf{e}}_\mathbf{y}\frac{\partial}{\partial y^*} + \hat{\mathbf{e}}_\mathbf{z}\frac{\partial}{\partial z^*}$, where $\hat{\mathbf{e}}_\mathbf{i}$ is the unit vector in the i direction. Since the Bingham model assumes the plug region to be a rigid body, the motion of the plug is governed by the rigid body dynamics. For stress $\boldsymbol{\tau}^*$, the Bingham constitutive relation is given by

$$\boldsymbol{\tau}^* = \eta^* \dot{\boldsymbol{\gamma}}^* \quad \text{for } \tau^* \geqslant \tau_0^*, \tag{2}$$

$$\dot{\boldsymbol{\gamma}}^* = 0 \quad \text{for } \tau^* < \tau_0^*, \tag{3}$$

where $\eta^* = \mu_0^* + \frac{\tau_0^*}{\dot{\gamma}^*}$ is the viscosity of the fluid with $\dot{\gamma}^* = [\dot{\gamma}_{ij}^* \dot{\gamma}_{ji}^*]^{1/2}$ the second invariant of the strain rate tensor. Here $\tau^* = [\tau_{ij}^* \tau_{ji}^*]^{1/2}$ and τ_0^* are, respectively, the second invariant of the stress tensor and yield stress. In the base state, at $y^* = R^*$, the no-slip assumption implies $\bar{v}_x^* = 0$, where an overbar signifies a base-state quantity. At the yielded-fluid–unyielded-fluid interface ($y^* = y_0 R^*$), Eq. (3) implies $\frac{d\bar{v}_x^*}{dy} = 0$. In the ensuing discussion, the dimensionless parameter $y_0 = \tau_0^*/\tau_w^*$ represents the extent of the unyielded-fluid region, with τ_w^* the shear stress at the wall in the base state. The flow is symmetric about the channel center and the plug region decouples the two yielded parts of the fluid. It should be noted that even after introducing perturbations, the assumption of the symmetry and decoupling of two parts remains valid as long as the plug region exists [2]. This further suggests that the limit of zero yield stress (or $y_0 \to 0$) is a singular limit, since there is an abrupt transition in the nature of boundary conditions from $y_0 \to 0$ to $y_0 = 0$. During the course of the present study, we have explicitly verified that even in the case of stability of Bingham flow in a rigid channel, the spectra for $y_0 \to 0$ and $y_0 = 0$ will be substantially different due to the discontinuous change in the boundary conditions. Interestingly, this feature is true even in the case of Bingham flow in rigid channels, but does not seem to have been explicitly discussed in the earlier literature [2,3,8,17,18]. Henceforth, we will consider only the upper half of the domain, i.e., $y \geqslant 0$. By using the above equations and boundary conditions, the steady-state, fully developed base-state velocity profile is given by

$$\bar{v}_x^* = \begin{cases} V_0^* & \text{for } 0 \leqslant y < y_0 R^* \\ V_0^*\left[1 - \frac{(y^* - y_0 R^*)^2}{(R^* - y_0 R^*)^2}\right] & \text{for } y_0 R^* \leqslant y < R^*, \end{cases} \tag{4}$$

where $V_0^* = \frac{R^* \tau_w^*}{2\mu_0^*}(1 - y_0)^2$ is the velocity of the unyielded plug. In the ensuing analysis, it is useful to carry out a coordinate transformation $y^* = y_0 R^* + \xi^*$. Thus, the velocity profile for the yielded zone becomes

$$\bar{v}_x^* = V_0^*\left[1 - \frac{\xi^{*2}}{(R^* - y_0 R^*)^2}\right]. \tag{5}$$

This expression shows that in order to obtain a familiar parabolic velocity profile similar to that of the plane Poiseuille flow of a Newtonian fluid, we must use $R^*(1 - y_0)$ and V_0^*, respectively, as length and velocity scales to nondimensionalize the governing equations. Similarly, pressure and stresses are nondimensionalized by $\mu_0^* V_0^*/[R^*(1 - y_0)]$. The dimensionless continuity equation is

$$\nabla \cdot \mathbf{v} = 0. \tag{6}$$

The dimensionless Cauchy momentum equation for the yielded region is

$$\mathrm{Re}\left[\frac{\partial \mathbf{v}}{\partial t} + (\mathbf{v} \cdot \nabla)\mathbf{v}\right] = -\nabla p + \nabla \cdot \boldsymbol{\tau}, \tag{7}$$

where $\mathrm{Re} = \rho^* V_0^* R^*(1 - y_0)/\mu_0^*$ is the Reynolds number. The Bingham model introduces one more dimensionless number, namely, the Bingham number B,

$$B = \frac{\tau_0^* R^*(1 - y_0)}{\mu_0^* V_0^*}. \tag{8}$$

As shown later on, the Bingham number and y_0 are related since both represent a nondimensional yield stress, and thus any one of these two can be chosen as an independent parameter. In the present analysis, y_0 is used as the measure of the yield stress. The constitutive equation in dimensionless form is

$$\boldsymbol{\tau} = \eta \dot{\boldsymbol{\gamma}} \quad \text{for } \tau \geqslant B, \tag{9}$$

$$\dot{\boldsymbol{\gamma}} = 0 \quad \text{for } \tau < B, \tag{10}$$

where $\eta = 1 + B/\dot{\gamma}$ is the dimensionless viscosity of the fluid.

The base-state velocity profile for the yielded region becomes

$$\bar{v}_x = 1 - \xi^2, \tag{11}$$

In this transformed coordinate ξ, the laminar base velocity profile in the yielded region takes the form of a parabolic profile in the domain $0 < \xi < 1$. Similarly, the base-state pressure gradient and the Bingham number in terms of y_0 are

$$\bar{p}(x) = -2x, \quad B = \frac{2y_0}{1 - y_0}. \tag{12}$$

For the solid, we consider a representative particle with position vector $\mathbf{X} = (X, Y, Z)$ in the undeformed state of the solid. On the undeformed solid, a stress field is induced due to flow driven by a pressure gradient in the flow direction. Due to the stresses, a deformation field is generated in the solid. In the deformed state, the representative particle assumes the position vector $\bar{\mathbf{x}} = (\bar{x}, \bar{\xi}, \bar{z})$. The position vectors in the current and undeformed configurations are related as $\bar{\mathbf{x}}(\mathbf{X}) = \mathbf{X} + \bar{\mathbf{u}}(\mathbf{X})$, where $\bar{\mathbf{u}}(\mathbf{X}) = (\bar{u}_x, \bar{u}_y, \bar{u}_z)(\mathbf{X})$ is the base-state displacement of the representative particle, with $\bar{u}_i(\mathbf{X})$ the components of the base-state displacement in the i direction. It should be noted that the nondimensionalization scheme and y-axis shift for the solid is similar to that employed for the fluid. The incompressibility condition for the solid is

$$\det(\bar{\mathbf{F}}) = 1, \tag{13}$$

where $\bar{\mathbf{F}} = \frac{\partial \bar{\mathbf{x}}}{\partial \mathbf{X}}$ is the base-state deformation gradient. The dimensionless governing equations and the Cauchy stress for a neo-Hookean solid for the steady base state are [12,19,20]

$$\nabla_{\mathbf{X}} \cdot \bar{\mathbf{P}} = 0, \tag{14}$$

$$\bar{\boldsymbol{\sigma}} = -\bar{p}_g \mathbf{I} + \frac{1}{\Gamma} \bar{\mathbf{F}} \cdot \bar{\mathbf{F}}^T, \quad \bar{\mathbf{P}} = \bar{\mathbf{F}}^{-1} \cdot \bar{\boldsymbol{\sigma}}, \tag{15}$$

where $\bar{p}_g$ and $\bar{\mathbf{P}}$ are, respectively, the base-state pressure acting on the solid on the deformed area and the first Piola-Kirchhoff stress tensor in the base state. The dimensionless parameter $\Gamma = \mu_0 V_0/[GR(1 - y_0)]$ can be interpreted as the dimensionless velocity of the plug region. To obtain the base state for the solid, the above base-state governing equations can be solved by using the following boundary conditions. Assuming a neo-Hookean solid to be perfectly bonded to a rigid solid at the dimensionless coordinate $\bar{\xi} = 1 + H$ implies $\bar{\mathbf{u}} = 0$, where $H = \tilde{H}/(1 - y_0)$. At the fluid-solid interface the velocity and stress continuities provide the remaining boundary conditions. We assume that the deformation of the solid is only in the flow direction; this is a reasonable assumption, considering the experimental conditions [15]. Hence, the base-state quantities for the solid in terms of the prestressed-state coordinates are

$$\bar{u}_x(\bar{\xi}) = \Gamma\{2y_0(1 + H - \bar{\xi}) + [(1 + H)^2 - \bar{\xi}^2](1 - y_0)\}, \quad \bar{u}_y(\bar{\xi}) = \bar{u}_x(\bar{\xi}) = 0, \tag{16}$$

$$\bar{p}_g(\bar{x}) = -2\bar{x}. \tag{17}$$

Next we impose infinitesimal two-dimensional perturbations on the above prestressed state. In general, we can consider three-dimensional perturbations, but as shown by Patne and Shankar [13],

for a Newtonian fluid flow past a deformable solid, two-dimensional disturbances are more unstable than the corresponding three-dimensional disturbances. Also, two-dimensional perturbations are less stable than corresponding three-dimensional perturbations for the plane Poiseuille flow of a Bingham fluid through a rigid channel [8]. Furthermore, as shown later, the Bingham fluid does not introduce any new interaction terms between the base-state and perturbed-state quantities in the solid governing equations or fluid-solid interface conditions in comparison with the Newtonian fluid, but merely changes the form of the base-state quantities which result in qualitatively different results. For these reasons, we expect two-dimensional perturbations to be more unstable than corresponding three-dimensional perturbations for the current system and thus assume two-dimensional perturbations in this study.

After the imposition of perturbations, the position vector of the representative particle is given by $\mathbf{x} = (x, \xi)$. This is related to the position vector of the particle in the prestressed state by the relation $\mathbf{x}(\bar{\mathbf{x}}) = \bar{\mathbf{x}} + \mathbf{u}'(\bar{\mathbf{x}}, \mathbf{t})$, where $\mathbf{u}'(\bar{\mathbf{x}}) = (u'_x, u'_y)(\bar{\mathbf{x}})$ is the Lagrangian displacement of the particle from its prestressed state with $u'_x(\bar{\mathbf{x}})$ and $u'_y(\bar{\mathbf{x}})$, respectively, as the x and y components of the displacement. The overall deformation gradient is $\mathbf{F} = \mathbf{F}' \cdot \bar{\mathbf{F}}$, where $\mathbf{F}' = \frac{\partial \mathbf{x}}{\partial \bar{\mathbf{x}}}$ is the perturbed-state deformation gradient. Thus, the incompressibility condition in the perturbed state is $\det(\mathbf{F}') = 1$. The dimensionless perturbed-state Cauchy stress tensor and the momentum balance equations are

$$\mathrm{Re}\frac{\partial^2 \mathbf{u}}{\partial t^2} = \nabla_{\bar{\mathbf{x}}} \cdot \mathbf{P}, \tag{18}$$

$$\boldsymbol{\sigma} = -p_g \mathbf{I} + \frac{1}{\Gamma}\mathbf{F} \cdot \mathbf{F}^T, \quad \mathbf{P} = \mathbf{F}'^{-1} \cdot \boldsymbol{\sigma}, \tag{19}$$

where $p_g = \bar{p}_g + p'_g$, with p'_g the perturbation in the pressure. The above equations for the fluid and solid are then linearized about the base state, and normal modes of the form

$$(v'_x, v'_y, p')(\mathbf{x}, t) = (\tilde{v}_x, \tilde{v}_y, \tilde{p})(\xi)e^{ik(x-ct)}, \tag{20}$$

$$(u'_x, u'_y, p'_g)(\bar{\mathbf{x}}, t) = (\tilde{u}_x, \tilde{u}_y, \tilde{p}_g)(\bar{\xi})e^{ik(\bar{x}-ct)} \tag{21}$$

are imposed, where k is the wave number in the x or $\bar{x}$ direction and takes only real values, while $c = c_r + ic_i$ is the complex speed of the perturbations. The base flow is temporally unstable if at least one eigenvalue satisfies the condition $c_i > 0$. The governing equations for the fluid side after simplification are

$$ik\tilde{v}_x + D\tilde{v}_y = 0, \tag{22}$$

$$\mathrm{Re}[ik(\bar{v}_x - c)\tilde{v}_x + D\bar{v}_x\tilde{v}_y] = -ik(1-y_0)\tilde{p} + (D^2 - k^2)\tilde{v}_x - \frac{2y_0k^2}{\xi(1-y_0)}\tilde{v}_x, \tag{23}$$

$$\mathrm{Re}[ik(\bar{v}_x - c)\tilde{v}_y] = -(1-y_0)D\tilde{p} + (D^2 - k^2)\tilde{v}_y + \left(\frac{2y_0}{\xi(1-y_0)}D^2 - \frac{2y_0}{\xi^2(1-y_0)}D\right)\tilde{v}_y, \tag{24}$$

where $D = \frac{d}{d\xi}$. Similarly for a solid, the governing equations are

$$ik\tilde{u}_x + D\tilde{u}_y = 0, \tag{25}$$

$$\begin{aligned} -k^2c^2\mathrm{Re}\tilde{u}_x &= -ik(1-y_0)^2\tilde{p}_g + \frac{1}{\Gamma}L^2\tilde{u}_x + 2D\tilde{u}_y, \\ -k^2c^2\mathrm{Re}\tilde{u}_y &= -(1-y_0)^2D\tilde{p}_g + \frac{1}{\Gamma}L^2\tilde{u}_y - 2D\tilde{u}_x, \end{aligned} \tag{26}$$

where $L^2 = D^2 - \frac{4ik\Gamma}{1-y_0}[y_0 + \bar{\xi}(1-y_0)]D - k^2 - \frac{4k^2\Gamma^2}{(1-y_0)^2}[y_0 + \bar{\xi}(1-y_0)]^2 - 2ik\Gamma$, with $D = \frac{d}{d\bar{\xi}}$. To solve these equations, we use following boundary conditions. In the base state, the plug region has thickness y_0 and the unperturbed interface is located at $\xi = 0$. However, due to the introduction of

the infinitesimal perturbations, there will be an infinitesimal change in the yielded region and hence the boundary conditions are to be derived at this new plug–yielded-fluid interface represented as

$$\xi = \epsilon, \tag{27}$$

where ϵ is the infinitesimal change in the thickness of the yielded region due to the presence of perturbations. The boundary conditions at the plug–yielded-fluid interface arise because (i) the stress is undefined in the plug region and from the Bingham fluid constitutive equation $\dot{\boldsymbol{\gamma}}(\bar{\mathbf{v}} + \mathbf{v}') = 0$ and (ii) the plug region is treated as a rigid body [2,8]. Thus, the boundary conditions at the plug–yielded-fluid interface are [2,8]

$$\tilde{v}_x = 0, \quad \tilde{v}_y = 0, \tag{28}$$

$$D\tilde{v}_x = -\tilde{\epsilon} D^2 \bar{v}_x|_{\xi=0}, \tag{29}$$

$$D\tilde{v}_y = 0, \tag{30}$$

where $\tilde{\epsilon}$ is the amplitude of the perturbation of the plug–yielded-fluid interface. Considering the four above boundary conditions along with the interface conditions, the problem may appear overspecified, but as discussed in the literature [17], the first two boundary conditions (28) are necessary for solving the eigenvalue problem. The other two boundary conditions are not directly used in solving the eigenvalue problem; instead, Eq. (29) is used for determining the amplitude of the perturbed interface ($\tilde{\epsilon}$) and Eq. (30) is necessary for the regularization of the momentum balance equations as $\xi \to 0$ [since the denominator term $\dot{\gamma}(\bar{v}_x) = D\bar{v}_x \to 0$ as $\xi \to 0$]. At $\xi = 1$, i.e., at the fluid-soft solid interface, the velocity and stress continuity give

$$\tilde{v}_y = -ikc\tilde{u}_y, \tag{31}$$

$$\tilde{v}_x - 2\tilde{u}_y = -ikc\tilde{u}_x, \tag{32}$$

$$\frac{1}{\Gamma} D\tilde{u}_x + \frac{ik}{\Gamma}\tilde{u}_y + 2\tilde{u}_y = (1 - y_0) D\tilde{v}_x + (1 - y_0) ik\tilde{v}_y, \tag{33}$$

$$-(1 - y_0)^2 \tilde{p}_g + \frac{2}{\Gamma}\left(D - \frac{2ik}{(1 - y_0)}\right)\tilde{u}_y - 2\tilde{u}_x = -(1 - y_0)^2 \tilde{p} + 2D\tilde{v}_y. \tag{34}$$

For the solid, at $\bar{\xi} = 1 + H$, i.e., where the deformable and rigid solids are perfectly bonded, the tangential and perpendicular displacements must vanish, and hence

$$\tilde{u}_x = 0, \quad \tilde{u}_y = 0. \tag{35}$$

The fluid governing equations (22)–(24) and the solid governing equations (25)–(27) are solved along with the boundary conditions (28), (31)–(34), and (35) to find the value of eigenvalue c by using either the shooting method or the pseudospectral method for fixed values of Re, y_0, H, k, and Γ.

Numerical methodology

In the pseudospectral method, we expand the perturbation quantities in terms of the Chebyshev polynomials as $\tilde{f}(\xi) = \sum_{n=0}^{n=N} a_n T_n(\xi)$, where $\tilde{f}(\xi)$, n, N, a_n, and $T_n(\xi)$ are, respectively, the perturbation quantity, the index for the Chebyshev polynomials, the highest degree of the polynomial in the series expansion, the coefficient of the nth polynomial, and the nth Chebyshev polynomial. We substitute the expansions in the linearized differential equations and require that the differential equation is exactly satisfied in N collocation points. The locations of the points are given by $\xi_n = \cos[\frac{n\pi}{N}]$. The resulting matrix problem is solved to obtain the eigenvalue c or the eigenfunctions in terms of the series coefficients a_n. The discretized matrices result in the following eigenvalue

problem:

$$c^2\mathbf{Ce} + c\mathbf{Be} + \mathbf{Ae} = 0. \tag{36}$$

Here **A**, **B**, and **C** are the discretized matrices and **e** is the eigenvector. To solve the above eigenvalue problem, we use the `polyeig` MATLAB routine. To remove the physically spurious eigenvalues, the code is executed for two different values of N (e.g., N and $N + 2$), and we filter physically genuine eigenvalues by setting a tolerance for comparison between the two spectra. The tolerance in our calculations was set to $O(10^{-5})$. The filtered eigenvalues are then given as initial guesses to the shooting code to validate the genuine nature of the eigenvalue.

To implement the shooting method, we integrate the domain from $\xi = 0$ up to the interface for the fluid and for the solid, from $\bar{\xi} = 1 + H$ up to the interface by using the `ode45` MATLAB routine, and then construct a square matrix of order 4×4 by using the interface conditions. The determinant of the resulting matrix is set to zero to determine the eigenvalue c. We use the result from the spectral computation as an initial guess for the Newton-Raphson iteration in the shooting procedure. If the shooting code converges to the eigenvalue after a finite number of iterations (usually 10–20), then it is regarded as the genuine eigenvalue.

III. RESULTS AND DISCUSSION

A. Results for Re = 0

Earlier work on the stability of plane Poiseuille flow of a Newtonian fluid through a neo-Hookean channel [13] predicted the presence of the short-wave instability alone for $\mathrm{Re} < 1$. The short-wave instability is characterized by $k_c > 2$ and $\Gamma_c > 1$ and is purely a consequence of the nonlinear solid model with a jump in the first normal stress difference across the fluid-solid interface [21]. However, plane Poiseuille flow of a Newtonian fluid through a neo-Hookean channel does not exhibit a finite-wave instability in the creeping-flow limit, when the consistent formulation is used for linearized interface conditions. The eigenmodes for the stability of the plane Poiseuille flow of a Newtonian fluid through a neo-Hookean channel can be divided into two classes of modes, depending on the symmetry of $\tilde{v}_y$ along the channel centerline, as varicose (odd) and sinuous (even) modes [22]. Both varicose and sinuous modes predict the same critical parameters for the short-wave instability. For the sake of comparison with Bingham fluid, we use the results for varicose modes.

The first question we address is whether a finite-wave-number instability is present in the creeping-flow limit for Bingham flow in a deformable channel. In marked contrast to its Newtonian counterpart, we find that plane Poiseuille Bingham flow in a deformable channel exhibits a finite-wave-number instability in the creeping-flow limit. For Newtonian fluids, only plane Couette flow exhibits this instability [13]. The presence of this finite-wave-number instability is demonstrated through the variation of c_i with k for the most unstable mode. Figure 2 compares c_i of the most unstable eigenvalue for the Newtonian and Bingham fluids and shows the presence of two types of instabilities for the Bingham fluid. Of these two instabilities, one becomes unstable for $k < 1$ and $\Gamma < 1$ [Fig. 2(a)] and shows characteristics similar to the finite-wave instability predicted for plane Couette flow past a deformable solid [23], while the other instability occurs for $k > 2$ and $\Gamma > 1$, which are characteristic of the short-wave instability shown in Fig. 2(b).

To ascertain the nature of the instabilities shown by the flow of a Bingham fluid through a neo-Hookean channel, we plot the neutral stability curves in k-Γ parameter space for fixed values of y_0 in Fig. 3. These plots show the critical wave number k_c and critical dimensionless speed of the plug $\Gamma_c < 1$, a characteristic of the finite-wave instability. Here Γ_c and k_c are, respectively, the lowest value of Γ at which flow becomes unstable and the wave number corresponding to Γ_c obtained from neutral stability curves in k-Γ space. Since the finite-wave instability is absent in plane Poiseuille flow of a Newtonian fluid through a neo-Hookean channel [11,24], the presence of the finite-wave instability is purely a consequence of the yield-stress nature of the fluid.

To understand the mechanism of the finite-wave instability predicted here, it is useful to examine the Bingham flow in a deformable channel in the limit $y_0 \to 0$, i.e., in the limit of vanishing

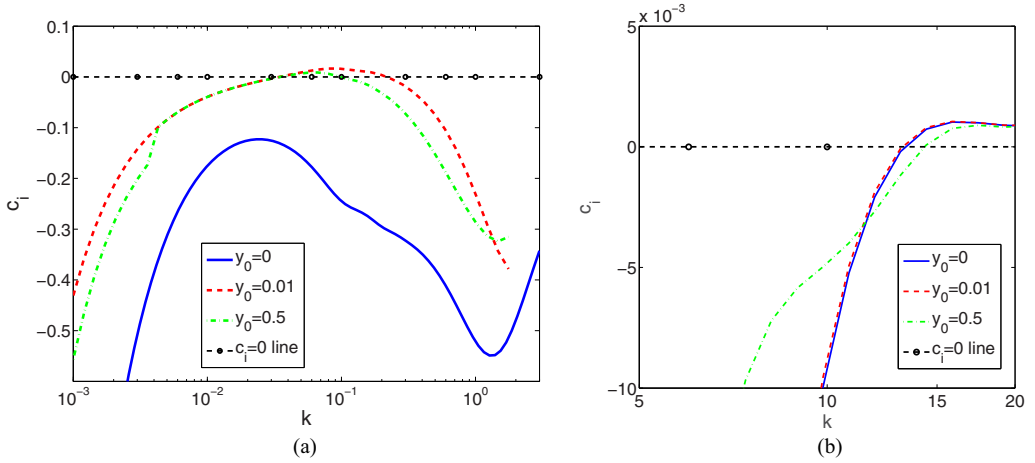

FIG. 2. Variation of c_i of the most unstable eigenvalue with k for $T = 0$ and $\mathrm{Re} = 0$. Here $y_0 = 0$ defines a Newtonian fluid (varicose mode). The presence of (a) finite-wave instability for $H = 10$ and $\Gamma = 0.5$ ($k < 1$) and (b) short-wave instability for $H = 0.1$ and $\Gamma = 2$ ($k > 5$) is shown for pressure-driven flow of a Bingham fluid in the creeping-flow limit.

but nonzero ratio of yield stress to shear stress at the wall. For a given yield-stress fluid and imposed pressure drop, the dimensionless ratio y_0 can be made much smaller than unity by changing the channel width. However, within the framework of linear stability analysis, the fluctuations are infinitesimal, and the neglect of nonlinear terms is not based on a controlled asymptotic approximation using a physical dimensionless small parameter (such as y_0). Thus, it is appropriate to first take the limit of infinitesimal perturbations and then consider the limit of $y_0 \ll 1$. In this limit, the thickness of the unyielded layer becomes very small compared to the half-channel height R^*. Yet the boundary conditions at the yielded-unyielded interface imply that the perturbation velocity fluctuations must go to zero, much akin to the scenario where a hypothetical rigid wall

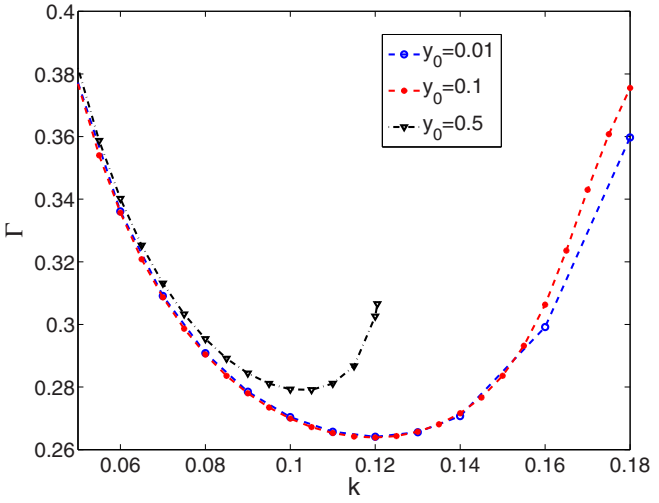

FIG. 3. Neutral stability curve in k-Γ space for $\mathrm{Re} = 0$ and $H = 10$. The figure shows the existence of the finite-wave instability for the Bingham fluid absent for the Newtonian fluid.

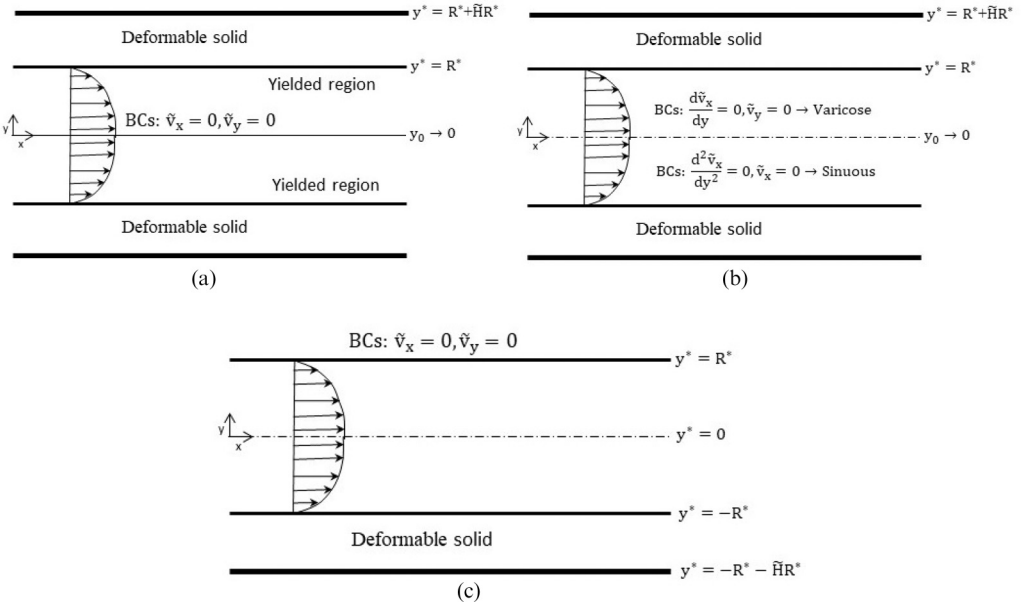

FIG. 4. (a) Reduction of the Bingham fluid problem to the plane Poiseuille flow with fictitious boundary conditions $\tilde{v}_x = \tilde{v}_y = 0$ at the channel centerline as $y_0 \to 0$. (b) Plane Poiseuille flow of a Newtonian fluid through a channel with both deformable walls with boundary conditions for varicose and sinuous modes at the channel centerline for $y_0 = 0$. (c) Plane Poiseuille flow of a Newtonian fluid with a deformable wall with no-slip and no-penetration boundary conditions at the upper plate.

is present at $y = 0$, schematically shown in Fig. 4(a). Thus, in the limit $y_0 \to 0$, the present problem reduces to plane Poiseuille flow of a Newtonian fluid through a neo-Hookean channel with fictitious boundary conditions $\tilde{v}_x = \tilde{v}_y = 0$ at the center of channel. We carry out the stability analysis for a pressure-driven flow of Newtonian fluid in a channel, but with fictitious no-slip boundary conditions at the channel centerline with $v_x = 0$ and $v_y = 0$. With these boundary conditions, we find that even the Newtonian flow is unstable in a neo-Hookean channel (Fig. 5), thus demonstrating the crucial role played by the boundary conditions. However, in the case of a true Newtonian flow in a channel [Fig. 4(b)], only conditions based on the symmetry or antisymmetry of the eigenfunctions are valid boundary conditions at the channel centerline. For a Bingham fluid, the no-slip conditions at the interface between yielded and unyielded regions emerge naturally. It should be noted that for arbitrary y_0, plane Poiseuille flow of a Bingham fluid does not reduce to plane Poiseuille flow of a Newtonian fluid with one deformable wall and another rigid wall as schematically shown in Fig. 4(c). This is because for plane Poiseuille flow of Bingham fluid boundary conditions, $\tilde{v}_x = \tilde{v}_y = 0$ are considered at the plug–yielded-fluid interface, which corresponds to the channel centerline as $y_0 \to 0$, while for plane Poiseuille flow of a Newtonian fluid with one deformable wall, the boundary conditions $\tilde{v}_x = \tilde{v}_y = 0$ are considered at the upper plate.

To further illustrate the importance of the boundary conditions, we consider plane Poiseuille flow of a Bingham fluid through a rigid channel with fictitious boundary conditions $\tilde{v}_x = \tilde{v}_y = 0$ at the center of channel. It is well known that plane Poiseuille flow of a Newtonian fluid exhibits Tollmien-Schlichting instability with a critical Reynolds number of 5772 which is also a sinuous mode of instability. The limiting case of Bingham fluid flow in a rigid channel with $y_0 \to 0$ is equivalent to a Newtonian flow in a rigid channel, but with no-slip conditions at the channel centerline. During the course of this study, we have found the latter to be linearly stable, unlike the true Newtonian channel flow, which is linearly unstable. Thus, the limit of vanishing yield stress is a singular limit, and it is not possible for the stability results to smoothly cross over from small values of y_0 to $y_0 = 0$.

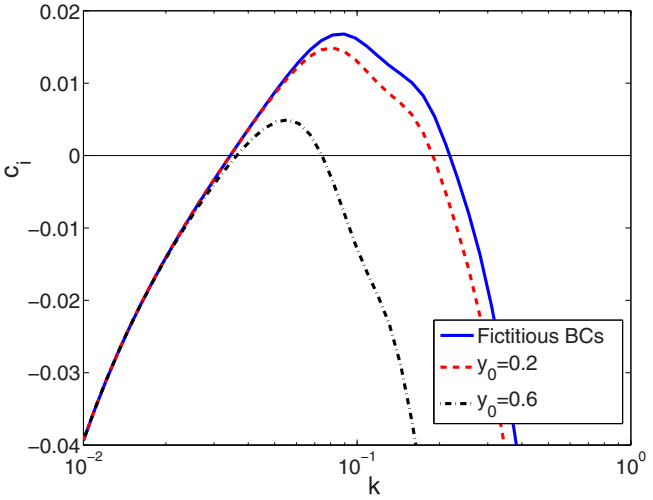

FIG. 5. Variation of c_i with k of the most unstable mode at Re $= 0$, $\Gamma = 0.5$, and $H = 10$. In the limit of $y_0 \to 0$, the finite-wave instability predicted here approaches the results for stability of plane Poiseuille flow of a Newtonian fluid with fictitious no-slip boundary conditions $\tilde{v}_x = 0$ and $\tilde{v}_y = 0$ at the channel centerline.

This observation, however, does not seem to have been made explicitly in prior literature on the stability of Bingham flow through rigid channels. The above discussion shows that the finite-wave instability exhibited by the plane Poiseuille flow of a Bingham fluid through a neo-Hookean channel is a consequence of the boundary conditions at the center of channel which arise naturally because of the interface between yielded and unyielded regions [2].

Experiments carried out for plane Couette flow of a Newtonian fluid past a deformable surface at low Re by Kumaran and Muralikrishnan [25] observed the presence of the finite-wave instability, in agreement with the theoretical predictions of Kumaran *et al.* [23]. Thus, it can be conjectured that the finite-wave instability predicted above for plane Poiseuille flow of Bingham fluids should also be observed experimentally. Furthermore, the experimental results of Kumaran and Muralikrishnan [25] were compared with theoretical predictions in the H-Γ_c parametric space. Hence, we plot the variation of Γ_c and k_c with H for three representative values of y_0. Figure 6 shows that the short-wave instability vanishes for sufficiently high values of y_0 and an increase in y_0 has a stabilizing effect on the finite-wave instability. The trend exhibited by the finite-wave instability can be explained with the aid of a simple scaling argument, which is based on earlier results for (Newtonian) plane Couette flow past a deformable solid. These studies have shown that the finite-wave instability occurs in a Newtonian fluid when the viscous stresses in the fluid are comparable to the elastic stresses in the deformable solid of a given thickness H:

$$\frac{\mu_0 V_0}{R(1-y_0)} \sim G \Rightarrow \frac{\mu_0 V_0}{R(1-y_0)} = \Gamma \sim O(1). \tag{37}$$

Furthermore, for a fixed value of y_0 and sufficiently high values of H, the above relation modifies to

$$\Gamma \sim \frac{\text{yielded-fluid thickness}}{\text{solid thickness}} \Rightarrow \Gamma \sim \frac{1}{H}. \tag{38}$$

This simple scaling argument explains the behavior exhibited in Fig. 6 for $H \gg 1$.

Figure 6 shows that the effect of an increase in y_0 on the short-wave instability is initially destabilizing, but a further increase in y_0 has a stabilizing effect. Also, experimentally, the pressure gradient is usually increased to probe the transition of the flow and in the present case from Eq. (17) the pressure gradient and y_0 are related. Thus, in Fig. 7(a) we plot the variation of Γ_c and k_c with y_0

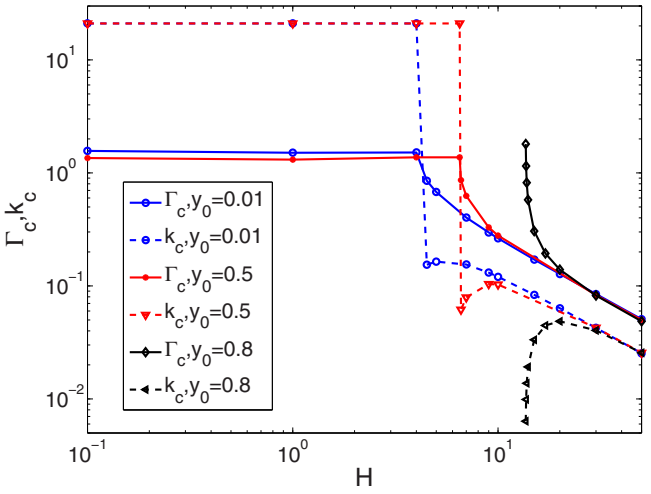

FIG. 6. Variation of Γ_c and k_c with H for $\mathrm{Re} = 0$. The finite-wave and short-wave instabilities are the critical modes of instability in $H > 1$ and $H < 1$ regions, respectively.

and find that the instability vanishes, for a fixed H, as $y_0 \to 1$. The data of Fig. 7(a) are then used to obtain Fig. 7(b), where we observe a collapse of the data for high values of H. The collapse of the data shown in Fig. 7(b) also affirms the scaling $\Gamma_c \sim 1/H$ for the finite-wave instability predicted here.

The stabilization predicted above for high values of y_0 can be explained as follows. In the present analysis, the dimensional solid thickness $\tilde{H}R$ is scaled with the thickness of the yielded fluid, viz., $R(1 - y_0)$. This yields $H = \tilde{H}/(1 - y_0)$, and for a fixed H, $\tilde{H} \to 0$ as $y_0 \to 1$, implying that the solid thickness is effectively decreasing in this limit. This leads to the stabilizing behavior exhibited in Fig. 7(a) as $y_0 \to 1$. However, if $\tilde{H}$ is fixed, then as $y_0 \to 1$, $H \gg 1$, and $\Gamma \sim 1/H \sim (1 - y_0)$ as shown in Fig. 8. Thus, the results in the limit of $H \gg 1$ or $y_0 \to 1$ are consistent with the proposed scaling argument.

Figure 9 shows the nonvanishing characteristic of the fluid eigenfunctions at $y = 1$, i.e., where the fluid–deformable-solid interface is present. It must be noted that for plane Poiseuille flow of a

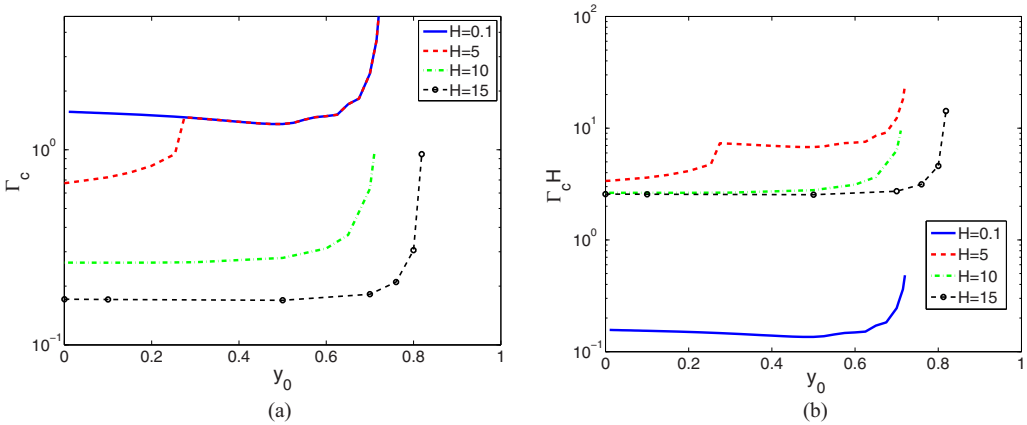

FIG. 7. (a) Variation of Γ_c with y_0. (b) Collapse of the data for $H = 10$ and 15 shows the existence of the scaling $\Gamma_c \sim 1/H$ for the finite-wave instability ($\Gamma_c H$ vs y_0).

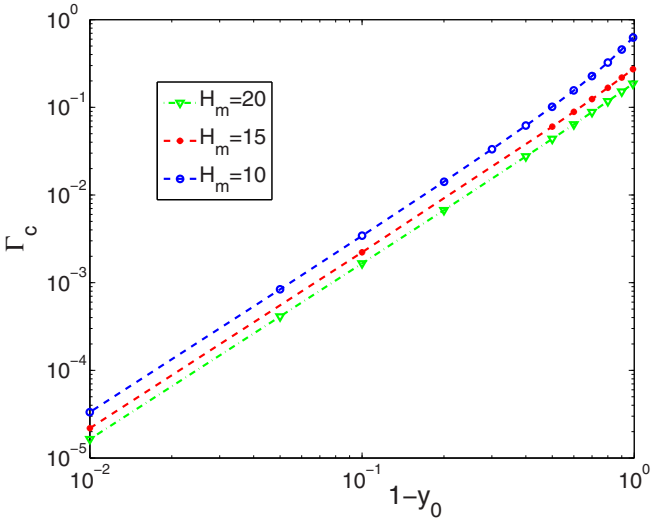

FIG. 8. Variation of Γ_c with y_0 for constant $\tilde{H} = (1 - y_0)H$ at $\mathrm{Re} = 0$. The figure shows scaling $\Gamma_c \sim (1 - y_0)$.

Bingham fluid past a rigid surface, the disturbances must vanish at $y = 1$. Thus, the nonvanishing characteristic shown in Fig. 9 is solely due to the presence of the deformable surface which leads to the exchange of the energy between the fluid and solid at the interface. This energy exchange occurs due to the interface conditions (31)–(34) which give rise to the instabilities predicted here.

B. Results for Re > 0

For $\mathrm{Re} < 1$ and H less than unity and/or for the values of y_0 for which finite-wave instability does not exist, the short-wave mode is the critical mode of instability. Figure 10 shows the variation

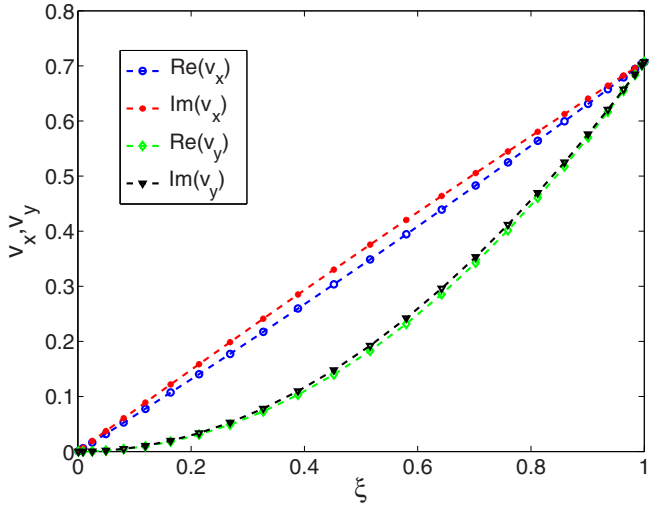

FIG. 9. Eigenfunction plots for the streamwise and normal components of the velocity for the neutrally stable eigenvalue $c = 0.950\,578$ obtained at $\mathrm{Re} = 0$, $H = 15$, $y_0 = 0.01$, $k = 0.0835$, and $\Gamma = 0.17141$.

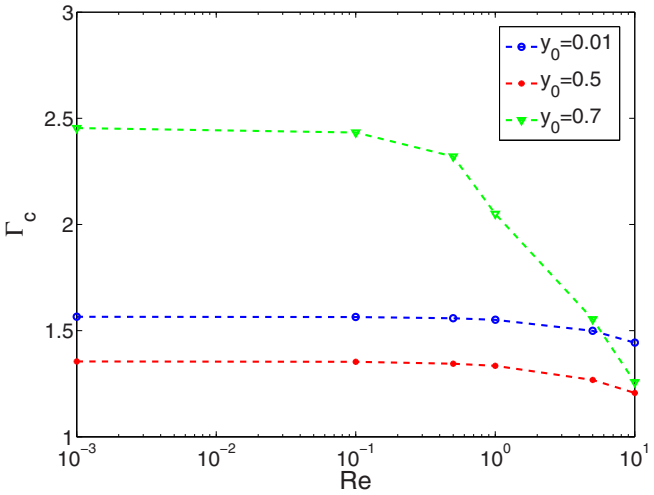

FIG. 10. Variation of Γ_c with Re at $H = 0.1$ for the short-wave mode. Increasing Re has a destabilizing effect on the short-wave instability.

of Γ_c with Re at $H = 0.1$ and shows the destabilizing effect of inertia on the short-wave mode. Additionally, from Fig. 10 we find that the increase in y_0 has an initial destabilizing effect, while a further increase in y_0 has a stabilizing effect, in agreement with the conclusions of Fig. 7(a). Furthermore, the destabilizing effect of inertia increases with increasing y_0. As shown later, for $\mathrm{Re} > 1$, other modes of the instability such as inviscid or wall modes dominate the short-wave mode. Furthermore, for $\mathrm{Re} > 10$, as k increases beyond 5, the number of collocation points required to accurately resolve the spectra increases; hence it is numerically difficult to track the short-wave mode at high Re. For this reason, we provide critical parameters for the short-wave mode for $\mathrm{Re} < 10$.

From the preceding discussion we can conclude that the finite-wave or short-wave instabilities dominate the stability behavior for $\mathrm{Re} < 1$ depending on the values of y_0 and H. For plane Poiseuille flow of a Newtonian fluid through a neo-Hookean channel, for $\mathrm{Re} > 1$, new modes of instability appear which can be classified into downstream ($c_r > 0$) and upstream ($c_r < 0$) traveling modes [13]. The upstream and downstream modes become, respectively, wall and inviscid modes when continued to high Re [13]. Figures 11(a) and 11(b) show the destabilization of the upstream modes for $y_0 = 0.01$ and $y_0 = 0.5$, respectively, with increasing Γ. With an increase in Re, new downstream modes are destabilized as shown in Fig. 12. In analogy with the Newtonian fluid [13], we anticipate that the mode may evolve into wall and inviscid modes at high Re depending on the sign of c_r. This expectation stems from the fact that at high Re the stability of the system is dominated by the inertial forces and viscous forces play a minor role.

In the preceding discussion we classified the instabilities and demonstrated the destabilization of downstream and upstream modes due to inertia. However, from an experimental point of view, it is the critical mode of the instability, i.e., the mode with minimum Γ_c, that is important. We next determine the critical parameters for the finite-wave, downstream, and upstream modes and compare them to obtain the most unstable mode to suggest the form of the instability that can be observed experimentally.

Figure 13(a) shows the variation of the critical parameters with Re for $y_0 = 0.01$ for the finite-wave mode. For $\mathrm{Re} > 10$, Γ_c for the finite-wave mode decreases as $\Gamma_c \sim \mathrm{Re}^{-1}$ while k_c approaches a constant value. The modes which show characteristic scaling $\Gamma_c \sim \mathrm{Re}^{-1}$ are classified as inviscid modes. For inviscid modes, inertial forces in the fluid and elastic forces in the solid balance each other, and thus $\rho V^2 \sim G$, which yields the scaling $\Gamma \sim \mathrm{Re}^{-1}$. In Fig. 12 we observed that with

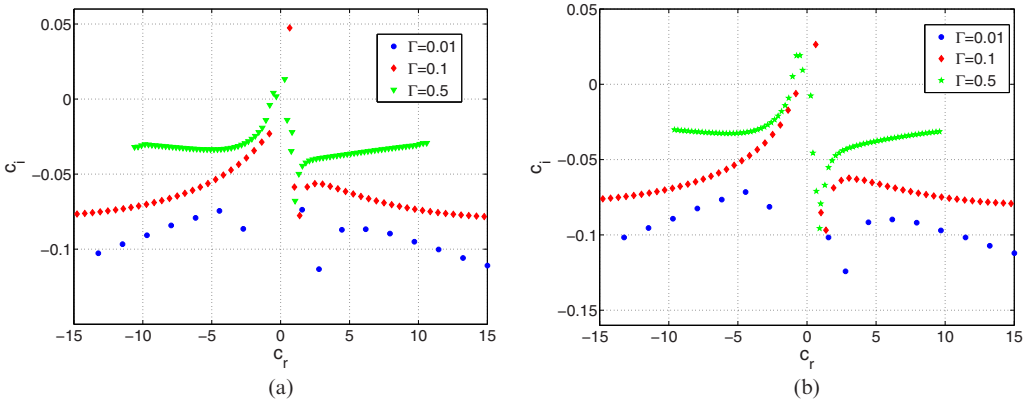

FIG. 11. Spectra showing the existence of upstream modes for Bingham fluid at (a) $y_0 = 0.01$ and (b) $y_0 = 0.5$. The other parameters utilized are $\mathrm{Re} = 50$, $k = 0.5$, and $H = 5$.

an increase in inertia, new downstream modes are destabilized, which hinted at the possibility of these modes being inviscid modes in analogy with the Newtonian fluid results. Figure 13(a) shows the most unstable downstream mode (other than the finite-wave mode) tracked at high Re and on expected lines, Γ_c for that mode decreases as $\Gamma_c \sim \mathrm{Re}^{-1}$, thereby showing that the downstream modes are inviscid modes.

Apart from inviscid modes, plane Poiseuille flow of a Newtonian fluid through a neo-Hookean channel exhibits another class of unstable modes. These modes originate from the fluid-solid interface due to the shear work done by the fluid on the solid and show characteristic scaling $\Gamma_c \sim \mathrm{Re}^{-1/3}$ at high Re. These modes are called wall modes in the literature [11,13] and form a characteristic wall layer near the fluid-solid interface where viscous and elastic forces balance each other. The upstream modes predicted in Figs. 11(a) and 11(b) are classified on the basis of Γ_c required to destabilize the mode. Thus, the first and the second wall mode respectively refer to the upstream modes with the lowest Γ_c and second lowest Γ_c. Figure 13(b) tracks the first two most unstable upstream modes for $y_0 = 0.01$ to high Re and shows that the modes show a characteristic

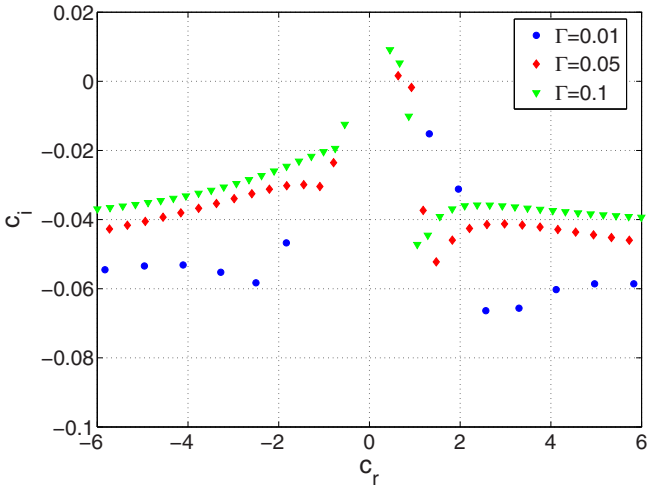

FIG. 12. Spectra showing the destabilization of downstream modes for Bingham fluid at $y_0 = 0.01$, $\mathrm{Re} = 50$, $k = 1$, and $H = 5$.

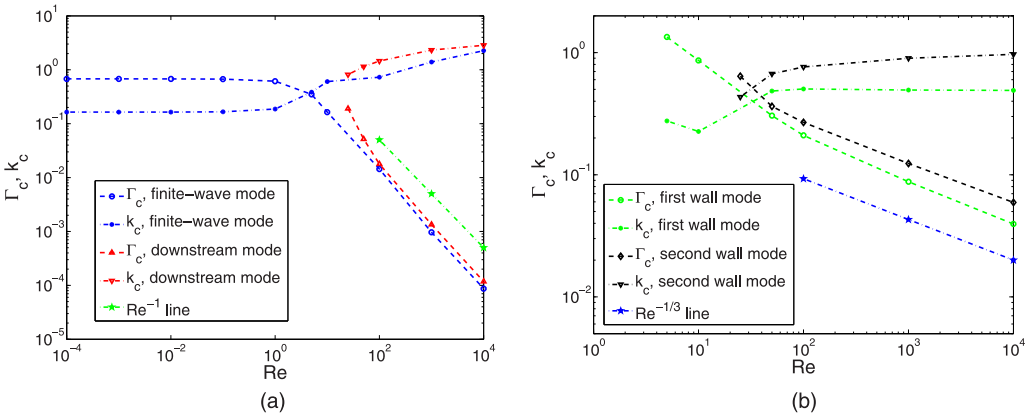

FIG. 13. Variation of critical parameters with Re at $H = 5$ and $y_0 = 0.01$ for (a) inviscid and (b) wall modes. The finite-wave mode is the most unstable inviscid mode while the first wall mode is the most unstable wall mode.

scaling $\Gamma_c \sim \mathrm{Re}^{-1/3}$ at high Re. Thus, the upstream modes destabilized due to inertia are a type of wall mode.

To ascertain the inviscid or wall mode nature of the eigenmodes, we plot the streamwise and normal components of the velocity eigenfunctions for the most unstable inviscid and wall modes at neutral stability points (i.e., $c_i \approx 0$) in Figs. 14 and 15. From Fig. 14 we see that the structure of the eigenfunctions for the inviscid mode is similar to that of a Newtonian fluid flow through a neo-Hookean channel [13]. The invariance in the structure of the eigenfunctions for the inviscid modes with change in the fluid is suggestive of the relatively minor role played by viscosity at high Re, since Bingham and Newtonian fluids differ in terms of the viscosity alone. Similar eigenfunctions for the streamwise and normal components of the velocity for the most unstable wall mode at the critical conditions are shown in Fig. 15. Unlike the inviscid mode, the wall mode eigenfunctions

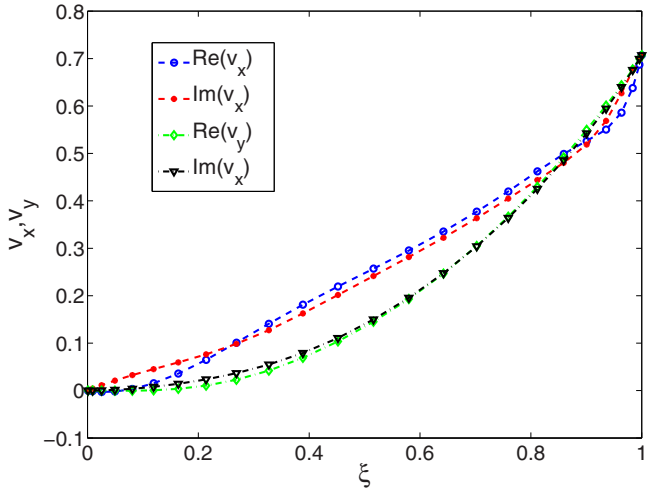

FIG. 14. Eigenfunction plots for the streamwise and normal components of the velocity for the neutrally stable eigenvalue $c \sim 0.953\,744 + 0i$ obtained at $\mathrm{Re} = 1000$, $H = 5$, $y_0 = 0.01$, $k = 1.392$, and $\Gamma = 0.000\,963\,5$.

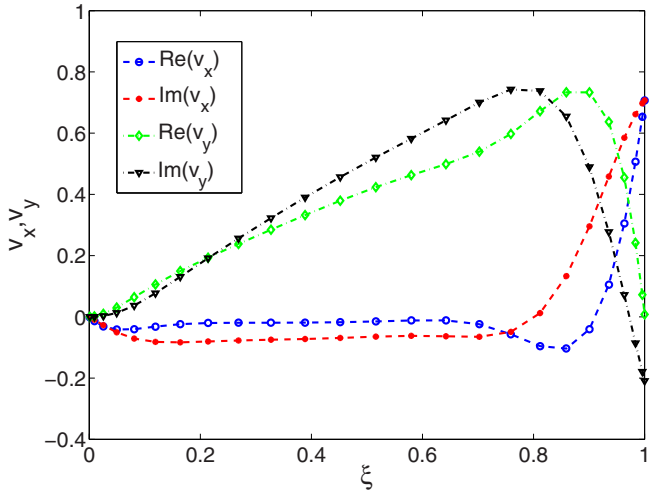

FIG. 15. Eigenfunction plots for the streamwise and normal components of the velocity for the eigenvalue $c \sim -0.201\,800 + 0i$ obtained at Re $= 1000$, $H = 5$, $y_0 = 0.01$, $k = 0.494$, and $\Gamma = 0.087\,67$. The maximum variation of the eigenfunctions near the deformable wall indicates the wall mode nature of the upstream mode.

show maximum variation near the deformable wall. This characteristic of maximum variation near the wall could be attributed to the formation of a viscous layer near the wall where viscous and elastic forces are comparable, which leads to the wall mode instability [26–29].

From Fig. 7(a) we observed that for $H = 5$, the finite-wave mode is stable for $y_0 > 0.25$, and thus the short-wave mode becomes the critical mode of instability. However, as shown in Fig. 16, the short-wave mode is not the critical mode of instability for Re > 5, because the downstream and upstream modes destabilized due to the inertia govern the stability of the system. Thus, for $5 <$ Re < 25 the first wall mode is the critical mode of instability, while for Re > 25 the inviscid

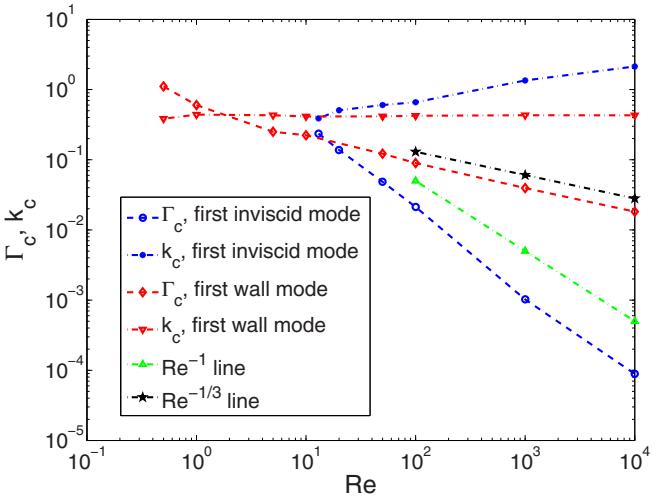

FIG. 16. Variation of critical parameters (Γ_c and k_c) with Re at $H = 5$ and $y_0 = 0.5$ for inviscid and wall modes. The inviscid and wall modes are, respectively, the critical modes of instability for Re < 10 and Re > 10.

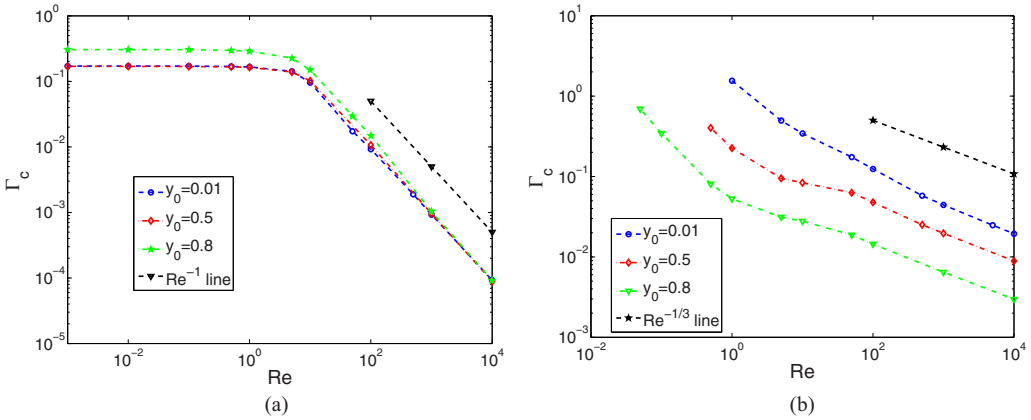

FIG. 17. Variation of Γ_c with Re at $H = 15$ for (a) finite-wave and (b) first wall modes. The finite-wave mode is the most unstable inviscid mode while first wall mode is the most unstable wall mode.

mode governs the stability of the system. To conclude, in the absence of the finite-wave instability, short-wave, wall mode, and inviscid modes of the instability determine the stability of the system in various ranges of Re, depending on the values of H and y_0.

In order to understand the change in the above stability picture with a change in the solid thickness, a similar analysis of the instabilities is carried out for $H = 15$ in Figs. 17(a) and 17(b). Figure 17(a) shows the variation in Γ_c with Re for the finite-wave mode for three values of y_0 since this is the most unstable downstream mode. We observe that at low Re, the curves for different plug thickness y_0 are separate provided y_0 is sufficiently high, but with an increase in Re the individual curves merge and show characteristic scaling of the inviscid modes. The merging of the curves observed at high Re is due to the dominance of the inertial forces over the viscous forces, thereby decreasing the influence of the viscosity variation with y_0.

Similarly, Fig. 17(b) shows the variation of Γ_c with Re for the first wall mode. Unlike finite-wave or downstream modes, the wall modes for different values of y_0 do not collapse on a single curve at sufficiently high Re. Rather, an increase in y_0 has a strong destabilizing effect on the wall modes, in contrast to inviscid modes. The lack of collapse of the curves for wall modes is due to the relatively high value of Γ_c required for the destabilization of wall modes, which can be explained as follows. The interaction terms between the base state and perturbed state introduced by the neo-Hookean model are proportional to the powers of Γ, and with a change in y_0, the solid base state changes [refer to Eq. (16)]. For an inviscid mode, a very low value of Γ_c undermines the effect of these interaction terms and inertia dominates the stability behavior. However, for the wall modes these interaction terms are sufficiently large to make a difference due to relatively high Γ_c. Hence, the curves for the inviscid mode at different y_0 collapse, while the curves for wall modes do not. In other words, even at high Re, for wall modes the influence of the viscosity remains large enough to affect their behavior.

Origin of the finite-wave mode

In Sec. III B we observed that if the finite-wave instability exists for a given y_0 and H in the creeping-flow limit, then it always continues to an inviscid mode at high Re. This gives rise to two possibilities at high Re: (i) A new mode originates due to fluid-deformable wall coupling and is destabilized due to the shear work done by the fluid at the fluid-solid interface and (ii) a mode that is already present in the spectra for the Bingham flow through a rigid channel is destabilized due to the introduction of the deformable solid.

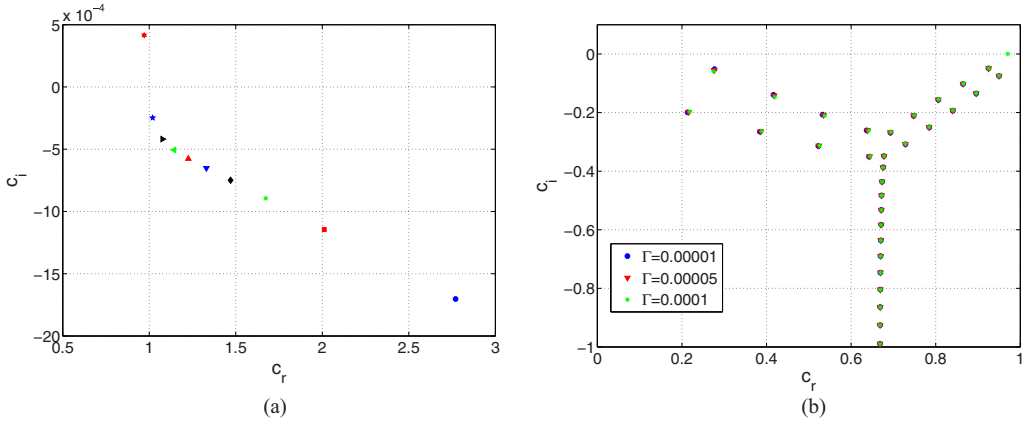

FIG. 18. Spectra at $\mathrm{Re} = 10^4$, $k = 1$, $H = 5$, and $y_0 = 0.01$ showing the destabilization of the inviscid modes of the Bingham fluid which manifests as finite-wave instability. (a) Destabilization of a downstream fluid-solid coupled mode which gives rise to the finite-wave mode with an increase in Γ. The eigenvalues are shown for $10^{-5} < \Gamma < 10^{-4}$ such that for each step Γ increases in steps of 10^{-5}. At $\Gamma = 10^{-5}$ the mode is stable (blue dot at $c \sim 2.75 - 0.0017i$); it moves towards the $c_i = 0$ line with increasing Γ and becomes unstable at $\Gamma = 10^{-4}$. (b) The invariable nature of the rigid spectra is shown with respect to variation in the deformability of the wall.

To determine the origin of the instability, in Fig. 18(a) we track the finite-wave mode by increasing Γ in steps of 10^{-5} and observe that the finite-wave mode originates from the fluid-solid coupled spectra and is not related to the spectrum of Bingham fluid in a rigid channel. To affirm the origin of the finite-wave mode and to understand the effect of deformability on the fluid spectra (present in a rigid channel), we plot [Fig. 18(b)] the variation of the fluid spectra with Γ. The invariance of the fluid spectra with change in Γ shows that the deformability of the channel wall does not have any effect on the fluid modes and the unstable modes are due to the coupling present in the system, thereby showing that the fluid-deformable wall coupling is responsible for the instabilities predicted in the present work.

C. Estimation for experiments

In this section we provide estimates for parameters wherein the instabilities can be observed in experiments using Carbopol solutions. For practical applications, where the properties of the fluid and deformable wall are specified, the above analysis is not directly applicable since both Re and Γ are dependent on the velocity. Thus, we define a flow-independent parameter $\Sigma = \mathrm{Re}/\Gamma = \rho^* G^* R^{*2}(1 - y_0)^2/\mu_0^{*2}$ and plot the variation of critical Re with Σ as shown in Figs. 19(a) and 19(b), respectively, for $y_0 = 0.01$, 0.5 and $H = 5$.

It is well known that the solutions of Carbopol in water exhibit yield stress [30–32]. To proceed further, we use the data for 0.6 wt.% Carbopol in water from Dinkgreve *et al.* [32]. In the earlier experiments on flow through a deformable channel, the channel half-height was of $O(10^2)$ μm, the shear modulus of the deformable channel was of $O(10^4)$ Pa, and the density $\rho^* \sim 10^3$ kg/m^3 [15]. For the fluid, the density of Carbopol solution $\rho^* \sim 10^3$ kg/m^3, the limiting viscosity range is $\mu_0^* \sim 0.1$–10^2 Pa s, and the yield stress is $O(10)$ Pa [32].

For these parameter values, Σ varies in the range $10(1 - y_0)^2$–$10^4(1 - y_0)^2$ corresponding to the range of the limiting viscosity. To estimate $y_0 = \tau_0^*/\tau_w^*$ for $\tau_0^* \sim 10$ Pa the driving pressure gradient may vary, which determines τ_w (which is proportional to applied pressure gradient), thereby determining y_0. For $y_0 = 0.01$, $\Sigma \sim 10$–10^4, which corresponds to a critical Reynolds number 4–115 from Fig. 19(a). Similarly, for $y_0 = 0.5$, $\Sigma \sim 2.5$–2500, which corresponds to a critical

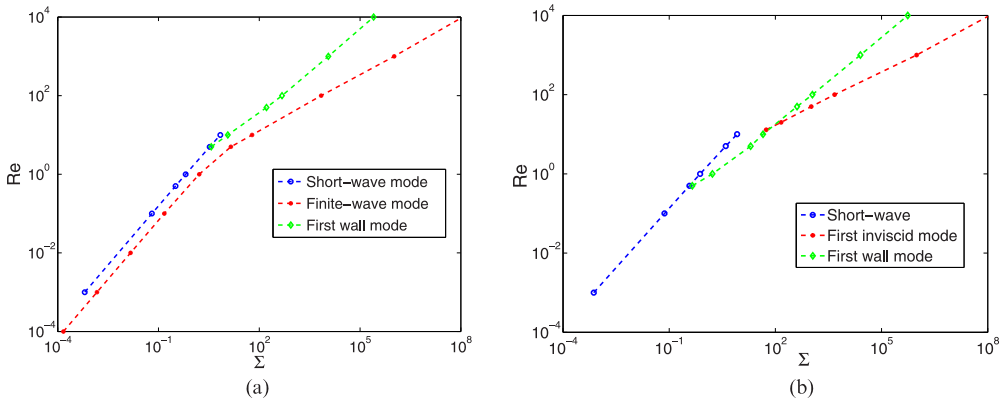

FIG. 19. Variation of critical Re with Σ for $H = 5$. For (a) $y_0 = 0.01$, the finite-wave mode is the critical mode, while for (b) $y_0 = 0.5$, the absence of the finite-wave mode makes short-wave, first inviscid, and wall modes critical modes of instability for different Re ranges.

Reynolds number of 3–75 from Fig. 19(b). The low Re at which instability is predicted to occur in a Bingham fluid makes future experimental investigations plausible.

IV. STABILITY OF THE PLANE POISEUILLE FLOW OF A BINGHAM FLUID WITH AN ELASTIC PLUG

The Bingham fluid model used thus far assumes a rigid plug before yielding and a Newtonian fluid after yielding as proposed originally by Bingham [6]. It is more realistic to treat the plug as an elastic solid before yielding. The elastic nature of the plug was identified and modeled for the first time by Oldroyd [7] by using a linear viscoelastic model for the plug. Thus, in this section we study the linear stability of the plane Poiseuille flow of a Bingham fluid through a rigid channel. The schematic of the geometry is the same as the one shown in Fig. 1, but with rigid walls instead of deformable walls.

Although Oldroyd [7] modeled the plug by using a linear elastic model, here we model the elastic plug using the purely elastic neo-Hookean model. The use of the neo-Hookean model is due to the availability of a consistent Eulerian formulation in the literature [13]. The Eulerian formulation is preferred for the elastic plug since the translational motion of the plug can be easily factored out in the formulation if we have an Eulerian frame of reference. Thus, we can concentrate only on the deformation in the solid which is of interest in the present work. The Bingham model with Oldroyd's correction, by using the nondimensionalization scheme outlined in Sec. II, in dimensionless form is

$$\boldsymbol{\tau} = -p_p \mathbf{I} + \frac{1}{\Gamma_p}(\mathbf{f}^T \cdot \mathbf{f})^{-1} \quad \text{for } \tau < B, \tag{39}$$

$$\boldsymbol{\tau} = \eta \dot{\boldsymbol{\gamma}} \quad \text{for } \tau \geqslant B, \tag{40}$$

where the subscript p signifies quantities defined for the plug region. The quantity $f = \frac{\partial \mathbf{X}}{\partial \mathbf{x}}$ is the deformation gradient in the Eulerian frame of reference, with $\mathbf{X}$ and $\mathbf{x}$ the coordinates of a particle in the undeformed and current state, respectively. In Eq. (39), p_p is the pressure field in the plug region and $\Gamma_p = \mu_0 V_0 / G_p R$ is the dimensionless plug velocity with G_p as the shear modulus of the plug. Thus, the plane Poiseuille flow of a Bingham fluid past a rigid surface is comprised of a coupled system with a yielded fluid and an elastic plug. In the following discussion we show that the consideration of an elastic plug instead of a rigid plug does not give rise to any new instability. This is accomplished by using the interface conditions between the yielded and unyielded regions.

We assume a representative particle in the undeformed state of the solid with position vector $\mathbf{X} = (X, Y, Z)$, and after deformation its position vector becomes $\mathbf{x} = (x, y, z)$. The position vectors of the particle in the two states are related by the relation

$$\mathbf{X}(\mathbf{x}) = \mathbf{x} - \mathbf{u}(\mathbf{x}), \tag{41}$$

where $\mathbf{u}(\mathbf{x})$ is the Eulerian displacement of the particle and it is specified by the motion describing the deformation. For the base state $\mathbf{u}(\mathbf{x}) = \bar{\mathbf{u}}(\mathbf{x})$, while for the perturbed state $\mathbf{u}(\mathbf{x}) = \mathbf{u}'(\mathbf{x})$.

As shown later, to understand the effect of consideration of an elastic plug, the exact form of the base state is not necessary. Two-dimensional infinitesimal perturbations are imposed on an arbitrary base state described as $\bar{v}_x = \bar{v}_x(y)$, $\bar{u}_x = \bar{u}_x(y)$, and a constant pressure gradient in the x direction, $d\bar{p}/dx = d\bar{p}_p/dx$. The infinitesimal perturbations are then assumed to take the normal modes of the form

$$(u'_x, u'_y, p'_p)(\mathbf{x}, t) = (\tilde{u}_x, \tilde{u}_y, \tilde{p}_p)(y)e^{ik(x-ct)}. \tag{42}$$

The plug-fluid interface is present at $y = y_0$; thus the base-state quantities required in the interface conditions need to be derived at the same location. The linearized interface conditions are

$$\tilde{v}_y = -ikc\tilde{u}_y, \tag{43}$$

$$\tilde{v}_x + (D\bar{v}_x)|_{y=y_0}\tilde{u}_y = -ikc[\tilde{u}_x + (D\bar{u}_x)|_{y=y_0}\tilde{u}_y], \tag{44}$$

$$\tilde{\tau}_{yx} = -ik(D\bar{u}_x)^2|_{y=y_0}\tilde{u}_y + \tilde{\sigma}_{yx}, \tag{45}$$

$$-\tilde{p} + \tilde{\tau}_{yy} = -\tilde{p}_g + \tilde{\sigma}_{yy}, \tag{46}$$

where $D = d/dy$ and $(.)|_{y=y_0}$ implies that the enclosed quantity should be evaluated at $y = y_0$. However, for a Bingham fluid (see Sec. II), $(D\bar{v}_x)|_{y=y_0} = 0$, and from interface conditions in the base state $(D\bar{u}_x)|_{y=y_0} = 0$. Thus, the above linearized interface conditions simplify to

$$\tilde{v}_y = -ikc\tilde{u}_y, \tag{47}$$

$$\tilde{v}_x = -ikc\tilde{u}_x, \tag{48}$$

$$\tilde{\sigma}^f_{yx} = \tilde{\sigma}_{yx}, \tag{49}$$

$$-\tilde{p} + \tilde{\sigma}^f_{yy} = -\tilde{p}_g + \tilde{\sigma}_{yy}. \tag{50}$$

An examination of these equations shows the absence of any term involving an interaction between the base state and perturbation quantities. The absence of these interaction terms precludes the coupling between the fluid and plug terms at the interface. It should be noted that the shear work done by the fluid at the fluid–deformable-solid interface causes the energy transfer from fluid to the deformable solid due to the fluid-solid coupling present at the interface and the energy so transferred is then returned to the fluid in a form that destabilizes the flow [25]. The same coupling [particularly the second term on the left-hand side of Eq. (44)] was the reason why Kumaran [33] predicted the finite-wave instability for the viscous plane Couette flow past a deformable solid. However, the absence of the coupling terms in the interface conditions obtained rules out any energy exchange mechanism thereby stabilizing the system. Thus, the plug and yielded regions are decoupled for the Bingham model with Oldroyd's correction. From the standpoint of linear stability analysis, this means that the stability of fluid flow in the yielded region is unaffected by the elastic nature of the plug.

For computational ease, regularized models, such as the Papanastasiou model [34], have been developed for which the yielded-fluid–plug-region interface does not have a discontinuity in the stress, unlike an ideal yield-stress fluid. The continuity introduced by the regularized models,

however, gives rise to a nonzero velocity gradient at the yielded-fluid–plug-region interface ($y = y_0$), depending on the parameters considered. Thus, if the parameter values are such that the velocity gradient is sufficiently high, then it may introduce a coupling between the base state and perturbations to result in an instability. A similar prediction regarding the parameter-dependent instability was made by Frigaard and Nouar [18] by carrying out a detailed linear stability calculation. They examined various viscosity regularization models for the Bingham fluid for predicting the hydrodynamic instabilities. The study of Frigaard and Nouar [18] concluded that the stability characteristics of the flow are incorrectly predicted by the use of viscosity regularization method models since the predicted instabilities are dependent on the parameters used in the models. In the present work, we reach the same conclusion, but using very general arguments.

V. CONCLUSION

In the present work we have analyzed the linear stability of plane Poiseuille flow of a Bingham fluid through a neo-Hookean channel. The analysis predicts the existence of the finite-wave instability in the creeping-flow limit that is absent for the plane Poiseuille flow of a Newtonian fluid through a neo-Hookean channel. The limiting case of a Bingham fluid with $y_0 \to 0$ shows that the finite-wave instability is due to the presence of the no-slip boundary conditions at the plug–yielded-fluid interface. Since the existence of the plug region is characteristic of the fluid model itself, it could be speculated that a similar finite-wave instability would be present for Bingham fluid flow through a neo-Hookean tube or past a neo-Hookean solid down an inclined plane.

The existence of the finite-wave mode is a function of y_0 and H such that an increase in y_0 and a decrease in H have a stabilizing effect. Additionally, we predicted the existence of a short-wave instability similar to Newtonian fluid flow past a deformable surface leading to the conclusion that the short-wave instability is an inherent feature of the neo-Hookean model as the instability originates from the jump in the first normal stress difference at the fluid-solid interface. Furthermore, at fixed H, an initial increase in y_0 has a destabilizing effect on the finite-wave mode, but higher values of y_0 have a stabilizing effect. The stabilizing effect on the instabilities with an increase in y_0 is due to the decrease in the effective thickness of the deformable solid.

For $\mathrm{Re} < 1$, the stability picture remains similar to the creeping-flow limit, but a further increase in Re gives rise to the destabilization of additional downstream and upstream modes. We computed the critical parameters for these unstable modes at increasing Re and found that the downstream and upstream modes belong to the class of inviscid and wall modes, respectively. At high Re, the continuation of the finite-wave mode shows scaling similar to an inviscid mode and has the lowest Γ_c among all inviscid modes, thereby becoming the most unstable inviscid mode. Furthermore, among all the inviscid and wall modes, if the continuation of the finite-wave mode to higher Re exists for a given value of H and y_0, then it is always the critical mode, i.e., the mode with the lowest Γ_c. In the absence of the finite-wave mode the short-wave, wall, and inviscid modes can be critical modes of the instability depending on y_0, Re, and H.

To study the effect of an elastic plug on the instabilities, we used the Bingham model with Oldroyd's correction. The analysis reveals that the dynamics of the plug and yielded regions is decoupled due to the vanishing of the velocity gradient at the plug–yielded-fluid interface for an ideal Bingham fluid. The regularized models, such as the Papanastasiou model, have nonzero values of the velocity gradient, which can give rise to spurious instabilities as these are dependent on the parameter values taken at the plug–yielded-fluid interface.

To summarize, the instabilities exhibited by plane Poiseuille flow of a Bingham fluid through a neo-Hookean channel are qualitatively different from those exhibited by a Newtonian fluid. Interestingly, the scenario in a deformable channel is just the opposite of what happens for Newtonian and Bingham flows in a rigid channel. For flow in a rigid channel, Newtonian flows are unstable but Bingham flows are stable, while the present study has shown that, for $\mathrm{Re} \ll 1$, Newtonian flow in a deformable channel is stable to finite-wavelength disturbances, but pressure-

driven flows of Bingham fluids are unstable. For biological fluid flows or flows of complex fluids with yield stress, the non-Newtonian character of the fluid must therefore be taken into consideration to understand the development of disturbances. The present study also provides estimates for parameter regimes under which the predicted instabilities can be realized in experiments.

ACKNOWLEDGMENT

The authors would like to thank B. Chandra and P. Joshi for instructive discussions.

[1] R. B. Bird, R. C. Armstrong, and O. Hassager, *Dynamics of Polymeric Liquids, Volume 1: Fluid Mechanics* (Wiley, New York, 1977).
[2] I. A. Frigaard, S. D. Howison, and I. J. Sobey, On the stability of Poiseuille flow of a Bingham fluid, J. Fluid Mech. **263**, 133 (1994).
[3] N. J. Balmforth, I. A. Frigaard, and G. Ovarlez, Yielding to stress: Recent developments in viscoplastic fluid mechanics, Annu. Rev. Fluid Mech. **46**, 121 (2014).
[4] C. Picart, J. M. Piau, H. Galliard, and P. Carpentier, Human blood shear yield stress and its hematocrit dependence, J. Rheol. **42**, 1 (1998).
[5] D. A. Fedosov, W. Pan, B. Caswell, G. Gompper, and G. E. Karniadakis, Predicting human blood viscosity in silico, Proc. Natl. Acad. Sci. USA **108**, 11772 (2011).
[6] E. C. Bingham, *Fluidity and Plasticity* (McGraw-Hill, New York, 1922), Chap. VIII, pp. 215–218.
[7] J. G. Oldroyd, A rational formulation of the equation of plastic flow for a Bingham solid, Proc. Cambridge Philos. Soc. **43**, 100 (1947).
[8] C. Nouar, N. Kabouya, J. Dusek, and M. Mamou, Modal and non-modal linear stability of the plane Bingham-Poiseuille flow, J. Fluid Mech. **577**, 211 (2007).
[9] P. G. Drazin and W. H. Reid, *Hydrodynamic Stability* (Cambridge University Press, Cambridge, 1981).
[10] V. Gkanis and S. Kumar, Stability of pressure-driven creeping flows in channels lined with a nonlinear elastic solid, J. Fluid Mech. **524**, 357 (2005).
[11] Gaurav and V. Shankar, Stability of pressure-driven flow in a deformable neo-Hookean channel, J. Fluid Mech. **659**, 318 (2010).
[12] R. Patne, D. Giribabu, and V. Shankar, Consistent formulations for stability of fluid flow through deformable channels and tubes, J. Fluid Mech. **827**, 31 (2017).
[13] R. Patne and V. Shankar, Stability of flow through deformable channels and tubes: Implications of consistent formulation, J. Fluid Mech. **860**, 837 (2018).
[14] M. K. S. Verma and V. Kumaran, A dynamical instability due to fluid-wall coupling lowers the transition Reynolds number in the flow through a flexible tube, J. Fluid Mech. **705**, 322 (2012).
[15] M. K. S. Verma and V. Kumaran, A multifold reduction in the transition Reynolds number, and ultra-fast mixing, in a micro-channel due to a dynamical instability induced by a soft wall, J. Fluid Mech. **727**, 407 (2013).
[16] R. Neelamegam, D. Giribabu, and V. Shankar, Instability of viscous flow over a deformable two-layered gel: Experiment and theory, Phys. Rev. E **90**, 043004 (2014).
[17] I. A. Frigaard and C. Nouar, On three-dimensional linear stability of Poiseuille flow of Bingham fluids, Phys. Fluids **15**, 2843 (2003).
[18] I. A. Frigaard and C. Nouar, On the usage of viscosity regularization methods for visco-plastic fluid flow computation, J. Non-Newtonian Fluid Mech. **127**, 1 (2005).
[19] G. A. Holzapfel, *Nonlinear Solid Mechanics* (Wiley, Chichester, 2000).
[20] C. W. Macosko, *Rheology: Principles, Measurements, and Applications* (Wiley-VCH, New York, 1994).
[21] V. Gkanis and S. Kumar, Instability of creeping Couette flow past a neo-Hookean solid, Phys. Fluids **15**, 2864 (2003).

[22] P. G. Drazin and L. N. Howard, in *Advances in Applied Mechanics*, edited by G. G. Chernyi (Academic, New York, 1966), Vol. 9, pp. 1–90.
[23] V. Kumaran, G. H. Fredrickson, and P. Pincus, Flow induced instability of the interface between a fluid and a gel at low Reynolds number, J. Phys. (France) II **4**, 893 (1994).
[24] R. Patne and V. Shankar, Absolute and convective instability in combined Couette-Poiseuille flow past a neo-Hookean solid, Phys. Fluids **29**, 124104 (2017).
[25] V. Kumaran and R. Muralikrishnan, Spontaneous Growth of Fluctuations in the Viscous Flow of a Fluid Past a Soft Interface, Phys. Rev. Lett. **84**, 3310 (2000).
[26] V. Kumaran, Stability of wall modes in a flexible tube, J. Fluid Mech. **362**, 1 (1998).
[27] V. Kumaran, Asymptotic analysis of wall modes in a flexible tube, Eur. Phys. J. B **4**, 519 (1998).
[28] V. Shankar and V. Kumaran, Asymptotic analysis of wall modes in a flexible tube revisited, Eur. Phys. J. B **19**, 607 (2001).
[29] V. Shankar and V. Kumaran, Stability of wall modes in fluid flow past a flexible surface, Phys. Fluids **14**, 2324 (2002).
[30] J.-Y. Kim, J.-Y. Song, E.-J. Lee, and S.-K. Park, Rheological properties and microstructures of Carbopol gel network system, Colloid. Polym. Sci. **281**, 614 (2003).
[31] P. C. F. Møller, A. Fall, and D. Bonn, Origin of apparent viscosity in yield stress fluids below yielding, Europhys. Lett. **87**, 38004 (2009).
[32] M. Dinkgreve, M. Fazilati, M. M. Denn, and D. Bonn, Carbopol: From a simple to a thixotropic yield stress fluid, J. Rheol. **62**, 773 (2018).
[33] V. Kumaran, Effect of fluid flow on the fluctuations at the surface of an elastic medium, J. Chem. Phys. **102**, 3452 (1994).
[34] T. C. Papanastasiou, Flows of materials with yield, J. Rheol. **31**, 385 (1987).